MITSUBISHI HEAVY INDUSTRIES, LTD.
16-5, KONAN 2-CHOME, MINATO-KU
TOKYO, JAPAN

July 13, 2010

Document Control Desk
U.S. Nuclear Regulatory Commission
Washington, DC 20555-0001

Attention: Mr. Jeffrey A. Ciocco

Docket No. 52-021
MHI Ref: UAP-HF-10201

Subject: **MHI's Responses to NRC's Request for Additional Information Technical Report CFD Analysis for Advanced Accumulator MUAP-09025**

Reference: [1] "Request for Additional Information Technical Report CFD Analysis for Advanced Accumulator MUAP-09025" dated May 14, 2010.
[2]" MHI's Responses to NRC's Request for Additional Information Technical Report CFD Analysis for Advanced Accumulator MUAP-09025", UAP-HF-10180, dated June 25

With this letter, Mitsubishi Heavy Industries, LTD. ("MHI") transmits to the U.S. Nuclear Regulatory Commission ("NRC") the document entitled "MHI's Responses to NRC's Request for Additional Information Technical Report CFD Analysis for Advanced Accumulator MUAP-09025" dated May 14, 2010.

Enclosed are the responses to No. 55 f) and 56 that are contained within Enclosure 2 and 3. The responses to No.54, 55 except 55 f) and 57 have been submitted in Reference [2].

As indicated in the enclosed materials, this document contains information that MHI considers proprietary, and therefore should be withheld from public disclosure pursuant to 10 C.F.R. § 2.390 (a)(4) as trade secrets and commercial or financial information which is privileged or confidential. A non-proprietary version of the document is also being submitted with the information identified as proprietary redacted and replaced by the designation "[ ]".

This letter includes a copy of the proprietary version (Enclosure 2), a copy of the non-proprietary version (Enclosure 3), and the Affidavit of Yoshiki Ogata (Enclosure 1) which identifies the reasons MHI respectfully requests that all materials designated as "Proprietary" in Enclosure 2 be withheld from public disclosure pursuant to 10 C.F.R. § 2.390 (a)(4).

Please contact Dr. C. Keith Paulson, Senior Technical Manager, Mitsubishi Nuclear Energy Systems, Inc. if the NRC has questions concerning any aspect of the submittal. His contact information is below.

Sincerely,

Y. Ogata

Yoshiki Ogata,
General Manager- APWR Promoting Department
Mitsubishi Heavy Industries, LTD.

D081
NRO

Enclosures:

1 - Affidavit of Yoshiki Ogata

2 - MHI's Responses to NRC's Request for Additional Information Technical Report CFD Analysis for Advanced Accumulator MUAP-09025 (proprietary)

3 - MHI's Responses to NRC's Request for Additional Information Technical Report CFD Analysis for Advanced Accumulator MUAP-09025 (non-proprietary)

CC: J. A. Ciocco
C. K. Paulson

Contact Information
C. Keith Paulson, Senior Technical Manager
Mitsubishi Nuclear Energy Systems, Inc.
300 Oxford Drive, Suite 301
Monroeville, PA 15146
E-mail: ckpaulson@mnes-us.com
Telephone: (412) 373-6466

ENCLOSURE 1

Docket No. 52-021
MHI Ref: UAP-HF-10201

MITSUBISHI HEAVY INDUSTRIES, LTD.

AFFIDAVIT

I, Yoshiki Ogata, state as follows:

1. I am General Manager, APWR Promoting Department, of Mitsubishi Heavy Industries, LTD ("MHI"), and have been delegated the function of reviewing MHI's US-APWR documentation to determine whether it contains information that should be withheld from public disclosure pursuant to 10 C.F.R. § 2.390 (a)(4) as trade secrets and commercial or financial information which is privileged or confidential.

2. In accordance with my responsibilities, I have reviewed the enclosed document entitled "MHI's Responses to NRC's Request for Additional Information Technical Report CFD Analysis for Advanced Accumulator MUAP-09025" dated July 2010, and have determined that portions of the document contain proprietary information that should be withheld from public disclosure. Those pages containing proprietary information are identified with the label "Proprietary" on the top of the page and the proprietary information has been bracketed with an open and closed bracket as shown here "[ ]". The first page of the document indicates that all information identified as "Proprietary" should be withheld from public disclosure pursuant to 10 C.F.R. § 2.390 (a)(4).

3. The information identified as proprietary in the enclosed document has in the past been, and will continue to be, held in confidence by MHI and its disclosure outside the company is limited to regulatory bodies, customers and potential customers, and their agents, suppliers, and licensees, and others with a legitimate need for the information, and is always subject to suitable measures to protect it from unauthorized use or disclosure.

4. The basis for holding the referenced information confidential is that it describes the unique design of the Advanced Accumulator developed by MHI and not used in the exact form by any of MHI's competitors. This information was developed at significant cost to MHI, since it required the performance of Research and Development and detailed design for its software and hardware extending over several years.

5. The referenced information is being furnished to the Nuclear Regulatory Commission ("NRC") in confidence and solely for the purpose of information to the NRC staff.

6. The referenced information is not available in public sources and could not be gathered readily from other publicly available information. Other than through the provisions in paragraph 3 above, MHI knows of no way the information could be lawfully acquired by organizations or individuals outside of MHI.

7. Public disclosure of the referenced information would assist competitors of MH in their design of new nuclear power plants without incurring the costs or risks associated with the design and testing of the subject systems. Therefore, disclosure of the information contained in the referenced document would have the following negative impacts on the competitive position of MH in the U.S. nuclear plant market:

A. Loss of competitive advantage due to the costs associated with development and testing of the Advanced Accumulator. Providing public access to such information permits competitors to duplicate or mimic the Advanced Accumulator design without incurring the associated costs.

B. Loss of competitive advantage of the US-APWR created by benefits of enhanced plant safety, and reduced operation and maintenance costs associated with the Advanced Accumulator.

I declare under penalty of perjury that the foregoing affidavit and the matters stated therein are true and correct to the best of my knowledge, information and belief.

Executed on this 13th day of July, 2010.

Yoshiki Ogata,
General Manager- APWR Promoting Department
Mitsubishi Heavy Industries, LTD.

Enclosure 3

UAP-HF-10201
Docket No. 52-021

MHI's Responses to NRC's Request for Additional Information

Technical Report CFD Analysis for Advanced Accumulator MUAP-09025

July 2010
(Non-Proprietary)

RAI for CFD Analyses for Advanced Accumulator, MUAP-09025-P (R0)

RAI 55.
The following items need further clarification regarding the MHI CFD results.

f) In the 2 cases (Test cases 3 and 6 in Table 3.4-1) MHI chose to analyze, please provide figures that can show when a cavitation starts and stops. In addition, please provide the actual values of void fraction in the vortex chamber for the small-flow regime.

Response

Figure 55-1 shows the cavitation starting point and ending point. In test Case6, cavitation process ends between [ ] seconds (cavitation factor equals to [ ] at this time) and [ ] seconds (cavitation factor equals to [ ] at this time).

The cavitation model in the FLUENT considers that vapor generates when local static pressure is less than the steam saturation pressure and that vapor condensates when local static pressure is larger than the steam saturation pressure. Equations for calculating vapor generation and condensation rates have been listed in Appendix-A. Steam saturation pressure evaluated by the FLUENT cavitation model is slightly higher than the user specified saturation pressure, since the model considers turbulence induced pressure fluctuations. Figure 55-2 plots void fraction and static pressure (absolute pressure) distributions at [ ] seconds in Case 6. The steam saturation pressure is not uniform in whole calculation domain due to turbulence induced pressure fluctuations (details have been shown in Appendix A). In this figure, regions where static pressure is lower than the steam saturation pressure have been marked and displayed. The figure shows that at [ ] seconds, static pressure at some locations near the throat has decreased to about [ ] Pa, which is lower than the steam saturation pressure. Cavitation occurs at these locations. Similarly, Figure 55-3 plots the void fraction and static pressure distributions at [ ] seconds in Case 6. In the technical report MUAP-09025, conditions at [ ] seconds have not been described for Case 6. At this time, detailed information at [ ] seconds was added in order to identify the stopping point of cavitation in Case 6. Figure 55-3 shows that the lowest static pressure at [ ] seconds is about [ ] Pa. Steam saturation pressure at the same location is lower than the static pressure by one order of magnitude. Thus, no cavitation occurs due to the fact that static pressure in whole calculation domain is higher than saturation pressure. Thus in Case 6, cavitation ends between [ ] seconds (cavitation factor equals to [ ]) and [ ] seconds (cavitation factor equals to [ ]).

The cavitation factor in whole time period of Case 3 is smaller than the cavitation factor at [ ] seconds in Test Case 6, thus, it is believed that cavitation occurs in all conditions for Case 3.
The DVD that has been sent to NRC contains void fraction data under small flow rate injection conditions. From these data, one can understand the void fraction distributions in the vortex chamber for small flow injection conditions.

Figure 55-1 Starting and Ending Points of the Cavitation Process

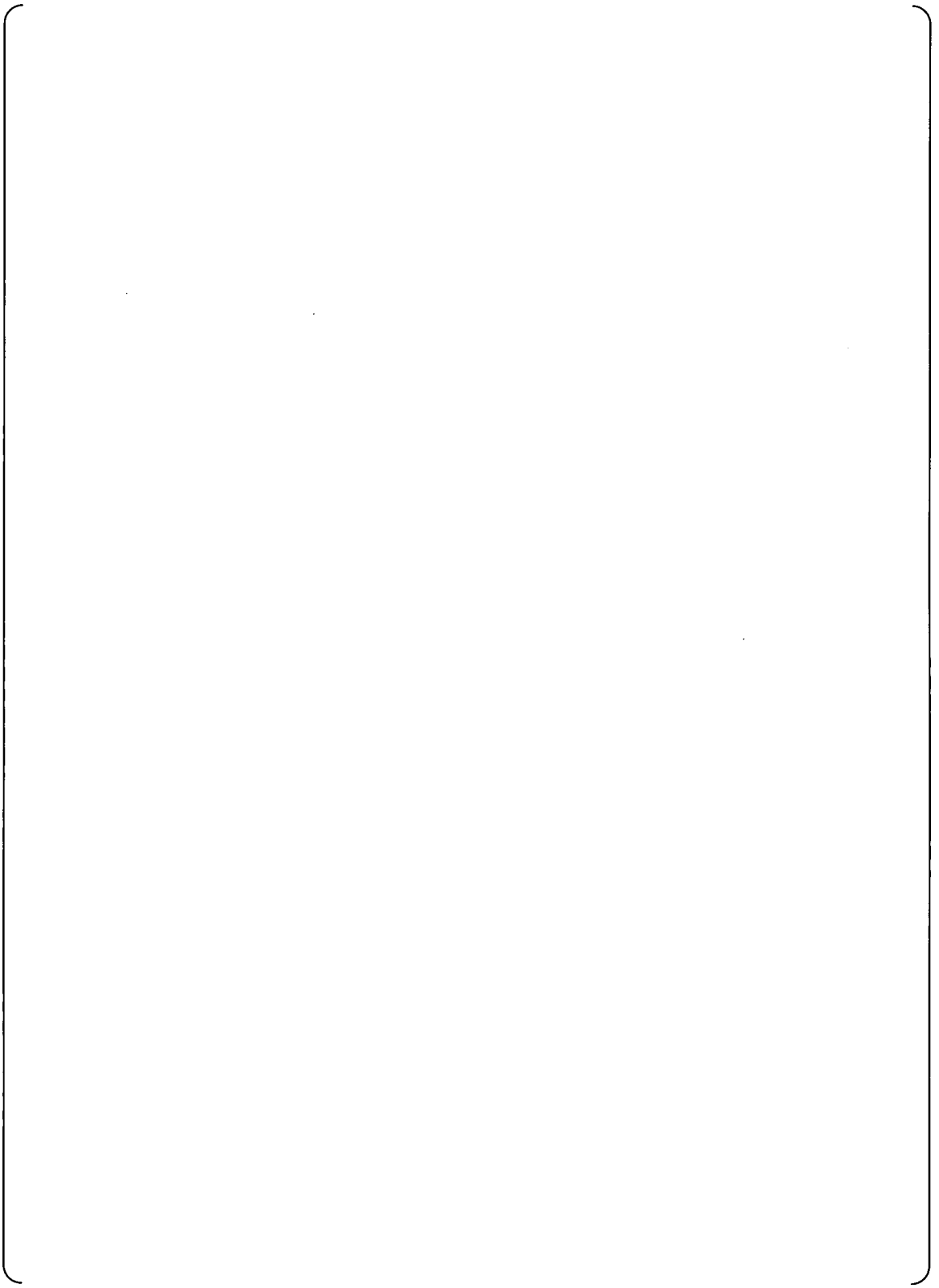

Figure 55-2 (1/2) CFD Simulation Results for Case 6 at [ ] Seconds

Figure 55-2 (2/2) CFD Simulation Results for Case 6 at [ ] Seconds

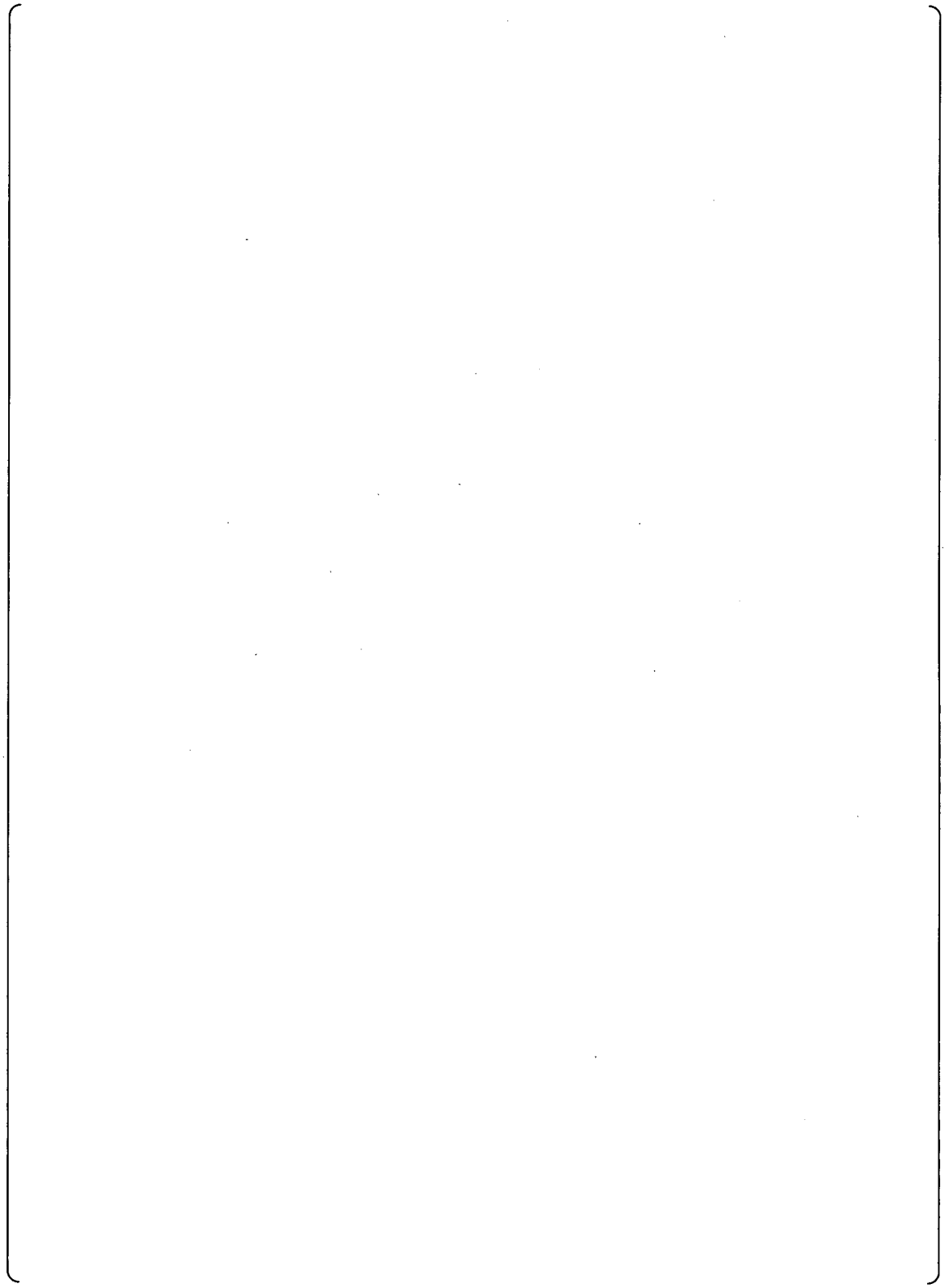

Figure 55-3 (1/2) CFD Simulation Results for Case 6 at [ ] Seconds

Figure 55-3 (2/2) CFD Simulation Results for Case 6 at [ ] Seconds

Appendix A

The cavitation model in the FLUENT uses following equations to calculate vapor generation/ condensation rates.

If $P < P_{sat}$

$$R_{evaporate} = 0.02 \frac{V_{ch}}{\sigma} \rho_l \rho_v \sqrt{\frac{2(P_{sat} - P)}{3\rho_l}} (1 - f)$$

If $P > P_{sat}$

$$R_{condensation} = 0.01 \frac{V_{ch}}{\sigma} \rho_l \rho_v \sqrt{\frac{2(P - P_{sat})}{3\rho_l}} f$$

Where

$R_{evaporate}$	: Vapor generation rate	P	: Local static pressure [Pa]
$R_{condensation}$	: Vapor condensation rate	P_{sat}	: Saturation pressure [Pa]
V_{ch}	: Characteristic velocity [m/s]	σ	: Surface tension [N/m]
ρ_l	: Density of liquid [kg/m^3]	ρ_v	: Density of vapor [kg/m^3]
f	: Vapor mass fraction [-]		

Turbulence-induced pressure fluctuation has been accounted for by utilizing the following equation to raise the saturation pressure.

$$P_{sat} = P_v + \frac{0.39}{0.5} \rho k$$

P_v : User specified saturation pressure [Pa]
ρ : Mixture density [kg/m^3]
k : Turbulent energy [m^2/s^2]

The FLUENT manual recommends including a small amount of non-condensable gases in the working fluid in order to enhance the numerical stability. In cases that small amount of non-condensable gases present in the working fluid, small void fraction data will be included in the simulation results. However, we must notice that such void fraction comes from the specified non-condensable gases for improving the numerical stability, and it does not means cavitation has occurred. As what has been described in this report, we judge that cavitation occurs only when local static pressure is lower than saturation pressure.

RAI 56.

The following documents provide best practice guidelines for the CFD analyses of nuclear reactors:

- Assessment Of Computational Fluid Dynamics (CFD) For Nuclear Reactor Safety Problems, January 2008, JT03239346, NEA/CSNI/R (2007)13
- Best Practice Guidelines for the use of CFD in Nuclear Reactor Safety Applications, NEA/CSNI/R (2007)5, 15-May-2007
- Policy of Journal of Fluids Engineering of ASME about CFD analyses. (Journaltool.asme.org/Content/JFENumAccuracy.pdf)

a) Were these best practices used in the MHI's CFD analyses?

b) Per the best practice guideline, the results of CFD analysis should include an estimate of numerical uncertainty and grid convergence.

Please provide an estimate of numerical uncertainty in the MHI's CFD analyses results. Please also provide results of grid convergence analyses.

c) Have any sensitivity been performed concerning the following?
1. Turbulence Modeling
2. Boundary conditions
3. Grid independence and grid convergence results.
4. Was grid convergence Index (GCI) used to assess the uncertainty?
5. Sensitivity on order of magnitude (second order was used only in the momentum equation).
6. Sensitivity on the type of wall function (using y+)

Response

a) Our CFD analysis mainly follows the techniques that have been explained in the document "Best Practice Guidelines for the use of CFD in Nuclear Reactor Safety Applications, NEA/CSNI/R (2007)5, 15-May-2007". For the uncertainty evaluation process on spacial discretization method, we referred to the example that has been recorded in the document "Policy of Journal of Fluids Engineering of ASME about CFD analyses. (Journaltool.asme.org/Content/JFENumAccuracy.pdf)". The document "Assessment Of Computational Fluid Dynamics (CFD) For Nuclear Reactor Safety Problems, January 2008, JT03239346, NEA/CSNI/R (2007)13" mainly introduces the background of making the BPG, therefore, it is not used for the reference of technical contents.

The evaluation results have been recorded in RAI56-b) and c).

b) The grid convergence and numerical uncertainty of CFD analysis have been assessed by following the GCI method, which is explained in "Journal of Fluids Engineering Editorial Policy, Statement on the Control of Numerical Accuracy" (http://Journaltool.asme.org/Content/JFENumAccuracy.pdf). CFD solution error has been evaluated in a numerically reliable way by applying three different mesh sizes. This process will be explained in the following paragraphs.

Figure 56-1 and 56-2 show the numerical simulation model for Case3 of 1/2-scale model, at [ ] seconds under large flow rate injection conditions. Cavitation happens near the center of vortex chamber and in the outlet pipe. The grid resolution in these regions has been assumed to be a parameter, by considering that cavitation process will affect the flow coefficient. Simulation model in the technical report MUAP-09025 includes nearly [ ] cells for the center of vortex chamber and the outlet pipe. The mesh size in Figure 56-1 is [ ] times to that in the report, thus there are nearly [ ] cells in the same regions. On the other hand, coarse mesh has been displayed in the Figure 56-2. There are only about [ ] cells in the same regions, since mesh size in this case is [ ] times of that in the report.

Figure 56-3 and 56-4 show the numerical simulation model for Case3 of 1/2-scale model, at [ ] seconds under small flow rate injection conditions. Same as that under large flow rate injection conditions, the grid resolution near the center of vortex chamber and the outlet pipe has been assumed to be a parameter. Simulation model in the technical report MUAP-09025 includes nearly [ ] cells for the center of vortex chamber and the outlet pipe. The mesh size in Figure 56-3 is [ ] times to that in the report, thus there are nearly [ ] cells in the same regions. On the other hand, coarse mesh has been displayed in the Figure 56-4. There are nearly [ ] cells in the same regions, since mesh size in this case is [ ] times of that in the report.

Figure 56-5 plots the relationship between the mesh size and the value of flow coefficient Cv obtained under such mesh size. Table 56-1 summarizes the estimation on numerical uncertainties based on the GCI method. Under the large flow rate injection conditions, the numerical uncertainty of the value of Cv is [ ]. Under the small flow rate injection conditions, the numerical uncertainty of the value of Cv is [ ].

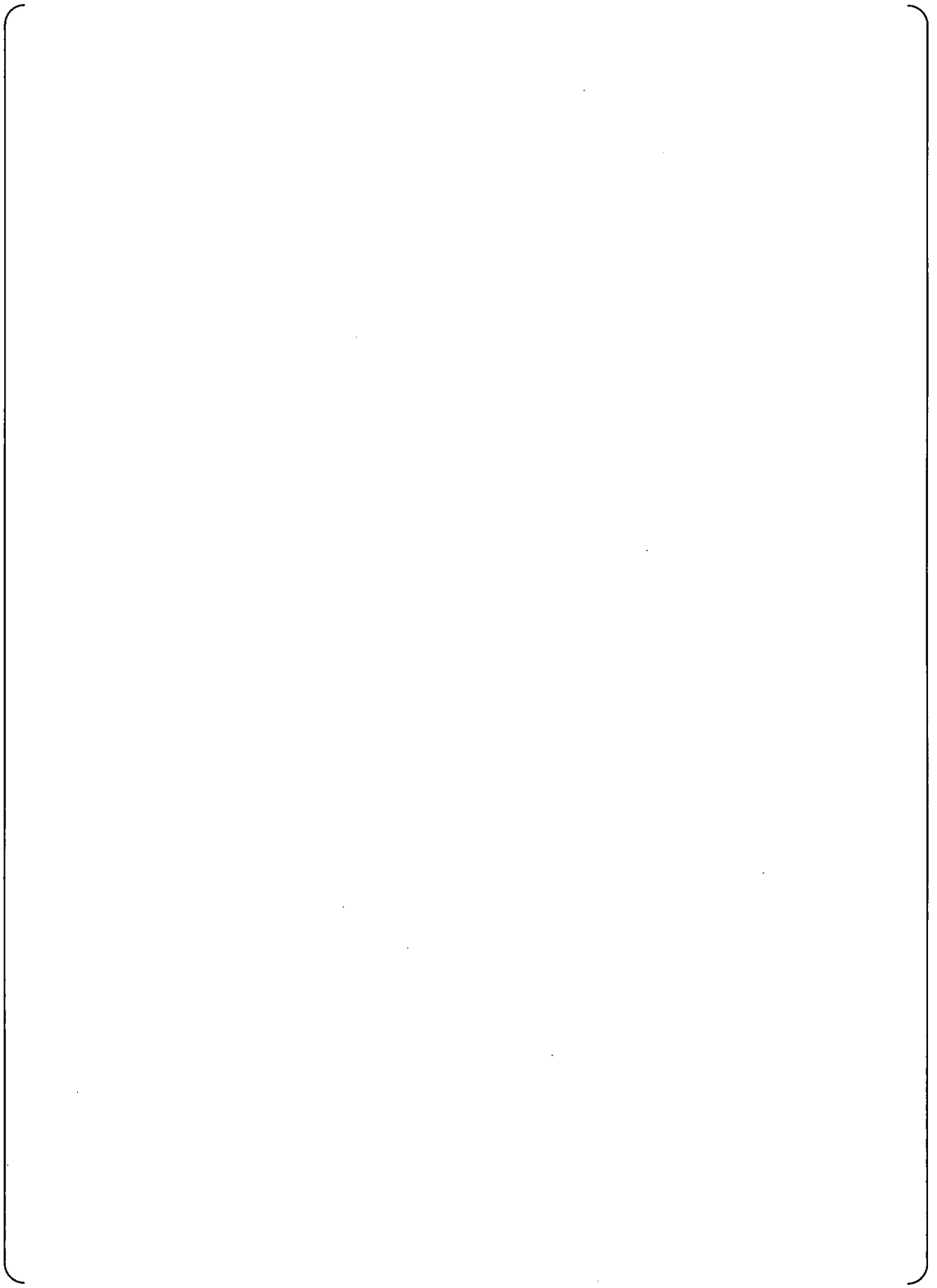

Figure 56-1 Mesh under large injection flow rate conditions (fine mesh)

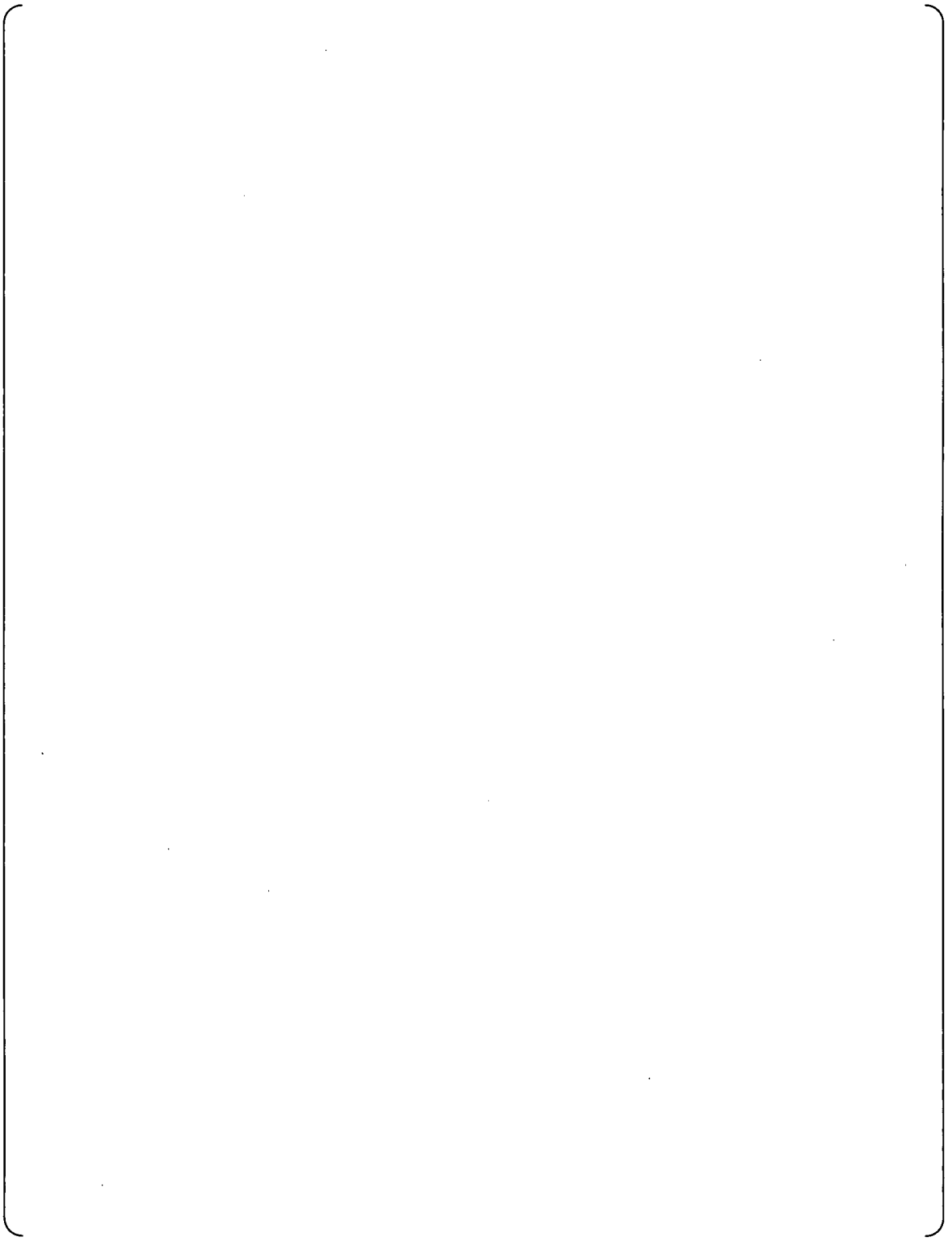

Figure 56-2 Mesh under large injection flow rate conditions (coarse mesh)

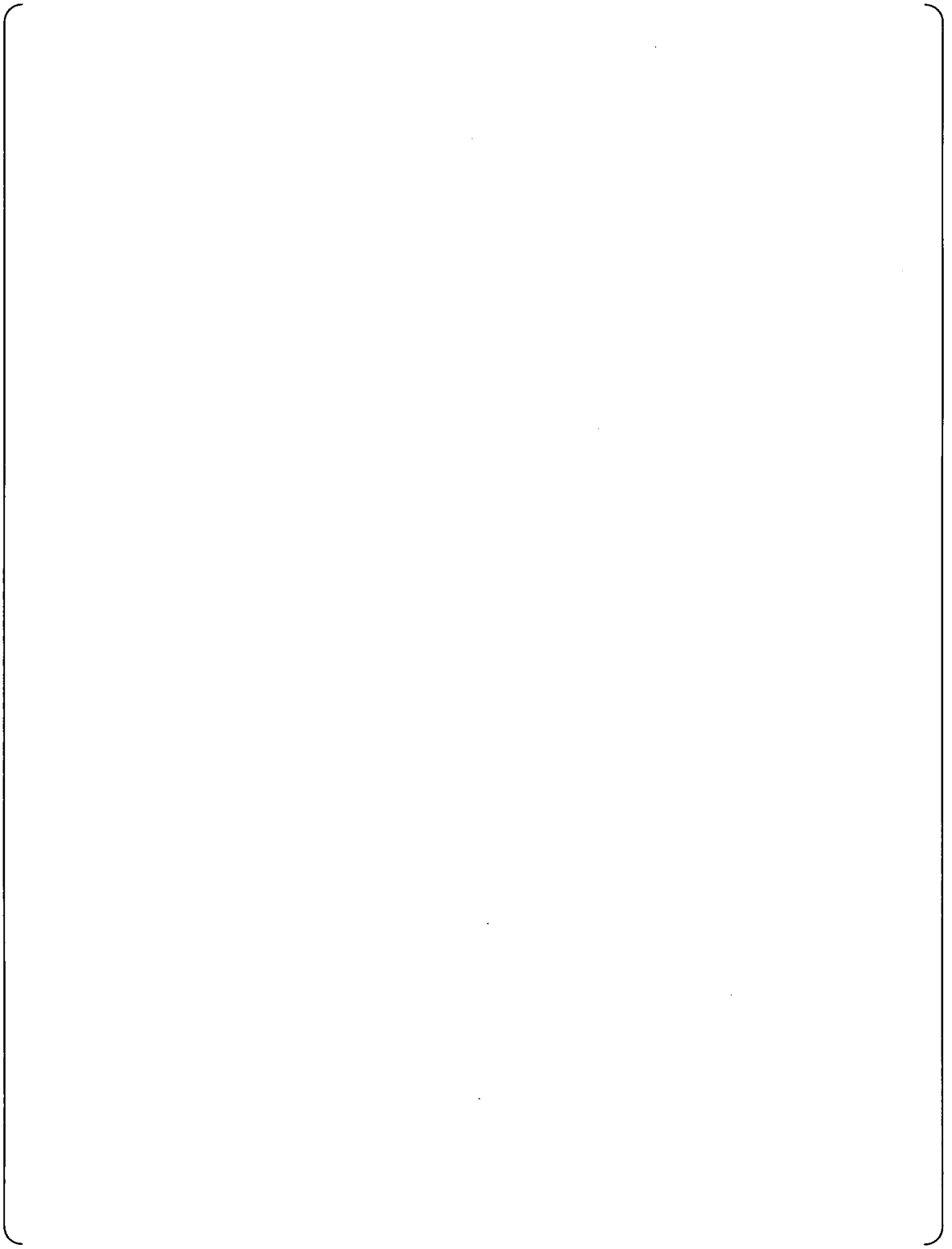

Figure 56-3 Mesh under small injection flow rate conditions (fine mesh)

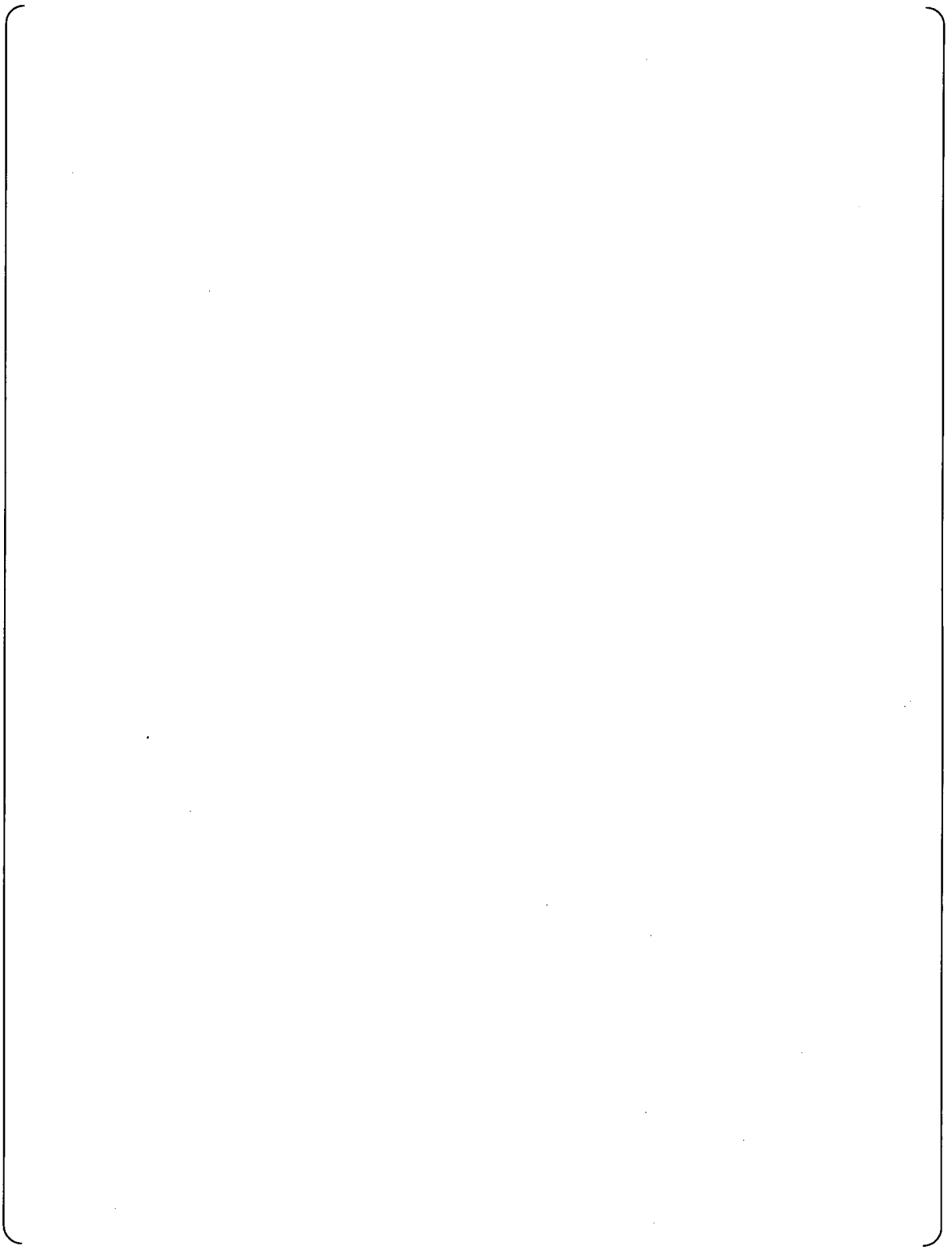

Figure 56-4 Mesh under small injection flow rate conditions (coarse mesh)

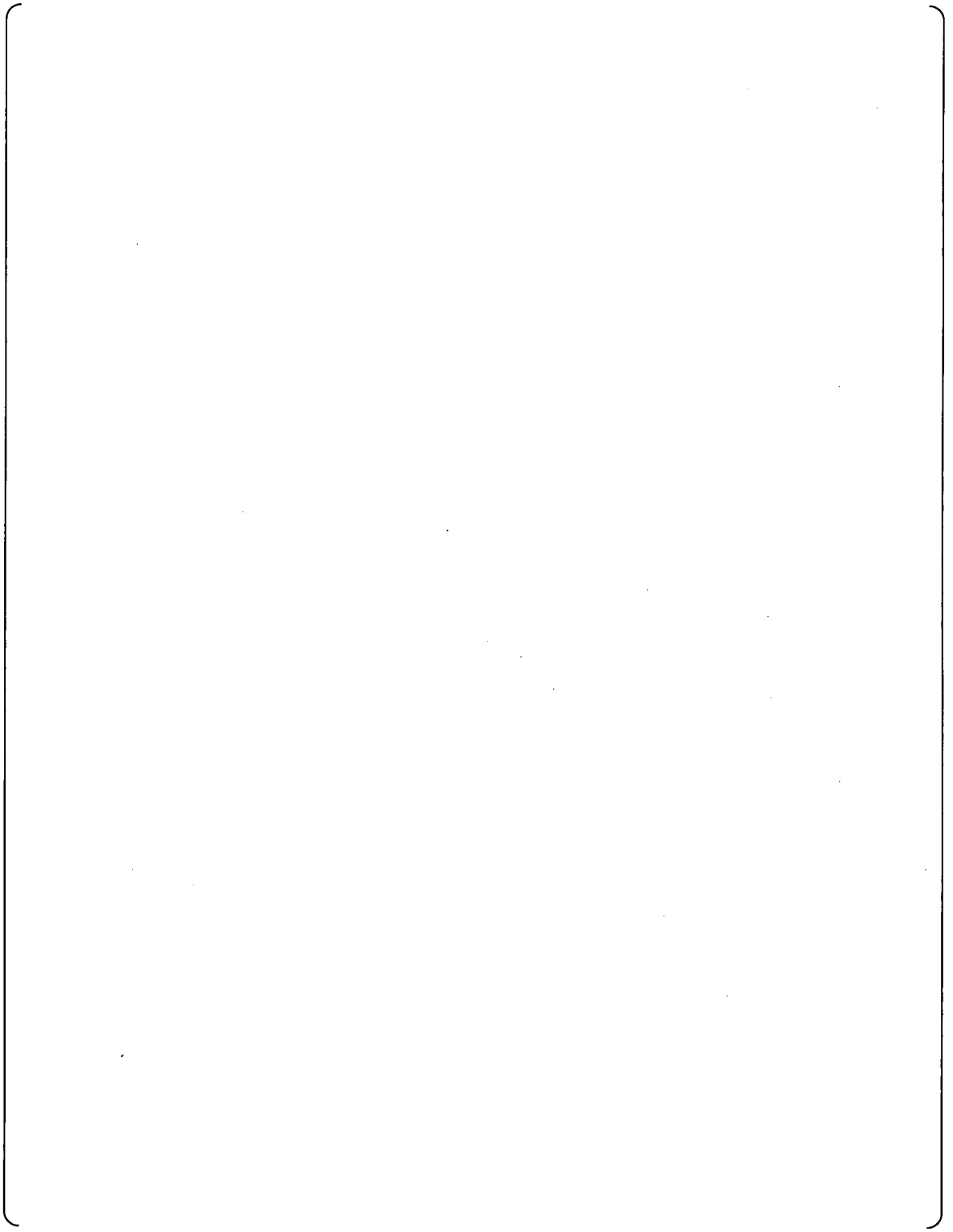

Figure 56-5 Evaluation on grid convergence

Table56-1 Evaluation on the Grid Convergence for Simulation Results

c)

1. In the flow field of the ACC, strong rotations exist in the vortex chamber. The RSM Model, which is the most suitable for the predictions on highly swirling flows among all available turbulence models in the FLUENT, has been applied in our CFD simulation. Due to the fact that all other turbulent models in the FLUENT are not suitable for our target highly swirling flow filed, we purposely did not perform the sensitivity study on turbulent modeling by evaluating the effects of different turbulence models on simulation results.

   Other choices of turbulence model (S-A model, k-ε model, etc.) are derived from the eddy viscosity model. They all apply the eddy viscosity approximation, which is not physically correct. Due to the limitation of the eddy viscosity approximation, the model accuracy in highly anisotropic flow field (i.e., high swirling flow) is low, and it tends to generate unjustified turbulence.

   On the other hand, the RSM model directly solves the transport equations for Reynolds stresses, thus it is a physically correct model.
   Therefore, compared with the eddy viscosity turbulence models, the RSM model is more effective for flows with highly anisotropic turbulence intensity, such as, swirling flows or boundary layer of rotation flow with strong Coriolis effect.

2. When boundary conditions are defined for the simulation, factors that affect the calculated internal flow field include the setup of the outlet boundary location. In the technical report MUAP-09025, the location of outlet boundary has been defined as the position of the pressure transducer that has been installed at downstream of the throat (10D from the elbow, D: pipe inner diameter). It is possible that flow separation and disturbances passing the elbow will propagate to this position, which might become one factor that influences the upstream flow. In order to avoid this effect, the location of outlet boundary has been moved to a further downstream position (16.3D from the elbow). It is expected that the flow is fully developed at this new position. The effects outlet boundary location on simulation results have been evaluated and confirmed. Figure 56-6 shows the simulation domain in our analysis.

   Table 56-2 summarizes the simulation results of Case3 at [ ] seconds under the large injection flow conditions. This table shows that different locations of outlet boundary will affect the prediction results. The difference between predicted Cv values is [ ]%. Figure 56-7 displays the flow fields at the outlet. This figure shows that the outlet flow does not include significant backflows, thus, it is concluded that the setup of different outlet boundary locations has a small impact on the flow field solution.

Table 56-2 Impact of Outlet Boundary Location

[ ]

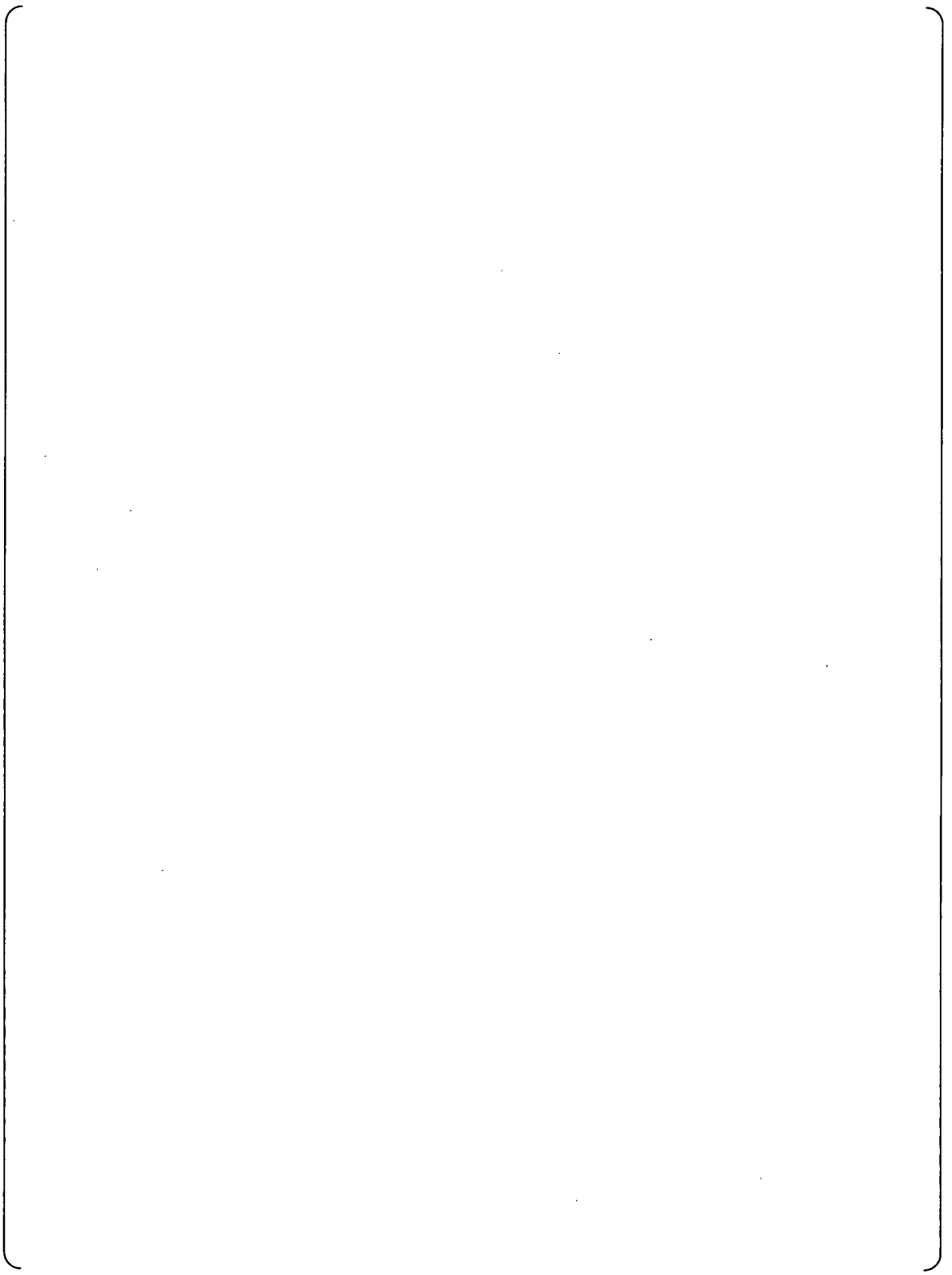

Figure 56-6 Model Figure

Figure 56-7 Flow conditions at the outlet (1/2-scale model, large injection flow rate conditions, Case 3, [ ] seconds)

3. As that has been answered in RAI56-b, the sensitive study has been performed.

4. As that has been answered in RAI56-b, the uncertainty has been evaluated by using the GCI.

5. This simulation requires to solve the momentum equation, transport equation of pressure terms, and transport equations of turbulence terms (for the RSM models). At first, the second-order discretization scheme has been chosen for all solved equations (momentum, pressure terms and turbulence terms). In case that the calculation is diverged under second-order schemes (Case No. 2 in the following table), sensitive evaluation for order of discretization scheme has been performed. The evaluation results are explained here.

   Therefore through sensitivity study, we found that converged results can not be reached once second-order scheme has been applied for the transportation equation for pressure term and turbulence term. Considering the results that have been summarized in Table 56-3, we applied the PREST! scheme and first-order scheme for the transportation equations of pressure term and turbulence term, in order to obtain converged solutions.
   (As that has been shown in No. 5, we also performed the calculation with first-order scheme for momentum equation. No influence on the value of Cv has been found in this calculation.)

Table 56-3 Sensitivity study on the order of discretization scheme

6. Issues that regard the choosing of wall function in the near wall regions have been discussed in the conference call on 7/9/2009.

   Since high Reynolds number flow exists in our simulation domain, plus that there are no obvious three-dimension effects near the wall, we can assume that local equilibrium has been established in this region. Thus, standard wall function has been utilized in our simulation (refer to supplemented material 1). On the other hand, the non-equilibrium wall function is recommended for simulation flows with separation, reattachment and impingement. Considering the fact that these phenomena only occur in a small region, their impacts on whole simulation domain are insignificant. Thus, the stand wall function has been utilized in this simulation. In addition, the grid specifications near the wall have already been checked with previous simulations. This grid have been prepared according to the FLUENT recommended method (refer to supplemented material 2).

   - Supplemented material 1 :

   Generally, following limitations should be considered when we apply standard wall function. However, in current simulations we did not encounter these limitations.

   - Can not assuming local equilibrium under following conditions
     - Large pressure gradient
     - Blowing/suction through the wall
     - Strong body forces
     - High three dimensionality in the near wall region
     - Sudden changes of fluid properties in the near wall region
   - For low Reynolds number flows(high viscosity, low velocity), the standard wall function can not be applied

   - Supplemented material 2 :

     Figure 56-8 shows the grid specifications near the wall and contour of the Y-plus. The figure shows that Y-plus near the vortex chamber wall is about [ ] under large injection flow rate conditions, and is between [ ] to [ ] under small injection flow rate conditions.

Figure 56-8 Supplemented material 2 (grid specifications near the wall and contour of the Y-plus)